Linear Forcing of Compressible Isotropic Turbulence in Rectangular Domains with Adapted Locally Refined Grids

Mario Sroka(✉) and Julius Reiss

Technische Universitaet Berlin, Mueller-Breslau-Strasse 15, 10623 Berlin, Germany
Mario.Sroka@tnt.tu-berlin.de, Julius.Reiss@tnt.TU-Berlin.DE

Abstract. This study investigates the applicability of the linear forcing method at rectangular domains with an adapted grid via local refinement. The advantages of the linear forcing method, using in a physical space solver for combustion simulations, are discussed. We present test cases for the different modifications of the forcing term and the major drawbacks occurring when using non-cubic domains. The use of a filtered velocity field within the forcing term is investigated, first as a solution for the described problems with rectangular domains and second as an attractive method to control the integral length scale of the turbulent field. Finally, we present results for various DNS computations in preparation for future studies of turbulence-flame interactions, and a few statistical properties of the turbulence are discussed.

Keywords: Compressible Navier-Stokes · Isotropic turbulence · Linear forcing · Adaptive locally refined block-structured grid · DNS

1 Motivation and Introduction

Flames are in most technical applications turbulent. The interaction between flames and turbulence is decisive for most of the flame properties. Thereby the study of this phenomenon is a central aspect of reactive flow research.

Previous investigations of a pulsed detonation combustor (PDC) at the TU Berlin revealed turbulence-flame interactions in an interesting and little-studied regime. [2] The turbulence is determined due to inflow conditions and geometry of the combustion chamber. A propagating flame creates a shock wave, which triggers the desired detonation in a focal point, making the turbulent flame acceleration decisive for the whole process. The oxygen-enriched hydrogen/air mixture combustion takes place under elevated pressure, and we observe a highly accelerated turbulent flame front. The strength of experimentally observed shock waves allows us to estimate the main properties of this strongly accelerated and compressible flame under elevated pressure. Note that the turbulence is not used to initialize the detonation (DDT), which is forced due to shock focusing.

A generic turbulent field needs to be produced and maintained with adequate parameters to investigate such turbulence-flame interactions numerically. The

R. King and D. Peitsch (Eds.): AFCC 2021, NNFM 152, pp. 187–202, 2022.
https://doi.org/10.1007/978-3-030-90727-3_12

characteristic turbulence parameters depend on the inflow conditions and the geometry of the combustor and are not fully known from the experiment.

If we take a look at a specific turbulent premixed combustion in the Borghi diagram (Fig. 1), we can that the two most important turbulent parameters are the RMS-velocity u_{rms} and the integral length scale l_t. In previous experiments, we observed a turbulent flame speed up to $50\frac{m}{s}$, which corresponds to an at least equal-sized RMS-velocity. For the cases from the experiments, the turbulence-flame interaction occurs at a turbulent Mach number of $\mathrm{Ma}_t = 0.12$ (for hydrogen/air mixture with equivalence ratio $\Phi = 1$ at $p = 1$ bar). Due to quenching effects, the RMS-velocity could even be much larger and exceed $\mathrm{Ma}_t > 0.12$. Under these conditions, the combustion will occur in the thin or broken reaction zone regime. Both regimes are from a numerical perspective interesting research areas. At higher pressures, the laminar flame speed increases while the flame thickness becomes smaller. This leads to a shifted (to the lower right corner) area of investigation in Fig. 1, but the above assumptions about the turbulent Mach number should be valid even for those cases.

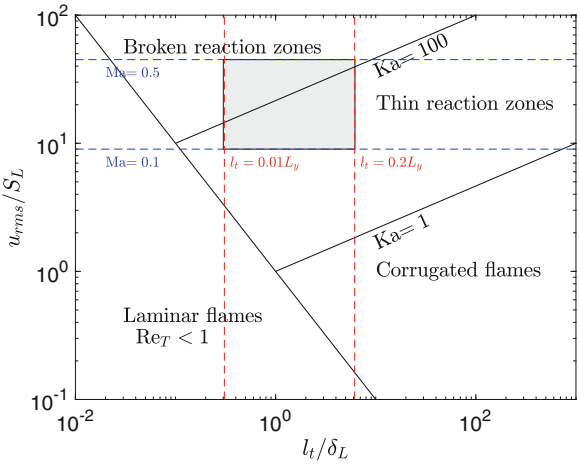

Fig. 1. Borghi plot to illustrate the area of investigation inside the premixed combustion diagram, fixed parameters for an example DNS computation: diffusive flame thickness δ_L and laminar flame speed s_L for a premixed H_2/air flame with equivalence ratio $\Phi = 1$ at $p = 1$bar, integral length scale l_t as part of the domain size $L_y = 2$ mm, turbulent Mach number is at least $\mathrm{Ma}_t = 0.1$

As mentioned, to investigate the turbulence-flame interaction at a specific point in the Borghi diagram, a turbulent field with a certain RMS-velocity and integral length scale is required. Therefore we need a turbulent forcing method capable of maintaining a turbulent field at these two parameters. Furthermore, the forcing method needs to work in the physical space because of the spatial formulation of our reactive DNS (direct numerical simulation) code. The utilization of locally adapted grids hinders the application of Fourier based methods.

For a Fourier transformation, we would have to interpolate the entire field to the finest grid level, which is prohibitive for high resolutions. And finally, the non-cubic domains cause difficulties in controlling the integral length scale, as discussed below.

A popular forcing method in physical space is proposed by Lundgren [11]. This method (Eq. 2) is easy to implement and depends only on local velocity values, which is a great advantage for adaptive meshes. Lundgren shows that his method is capable of computing statistically stationary turbulence with correct physical properties. Carroll and Blanquart [6] modified the linear forcing term to reduce fluctuations and therefore achieve a shorter transient time before getting statistically stationary turbulence. A further modification was proposed by Bassenne et al. [1] (Eq. 3). With this term, the statistically stationary state is reached even faster, and specific target values (turbulent kinetic energy or dissipation) can hold at nearly constant values. Similar to the original forcing term, it also works very well on adapted meshes. Global turbulence properties, used as inputs for this forcing term, can easily be computed on adapted grids with low computational costs. To summarize, the linear forcing can maintain specific turbulent kinetic energy (RMS-velocity), which is essential to research turbulence-flame interactions. In Sect. 3, we discuss the advantages and disadvantages of these different approaches for our specific problem.

The second important turbulent property is the integral length scale. Rosales and Meneveau [15] studied the differences between the linear forcing and the classical pseudospectral method. The pseudospectral forcing usually works with a band-limiting (low-wavenumber) approach, while the linear forcing term increases the turbulent kinetic energy at all wavenumbers. Rosales and Meneveau find that the integral length scale with Lundgren's method is approximately $l_t \approx 0.2L$ of the domain size L. Band-limited forcing yields $l_t \approx 0.4L$. Palmore and Desjardins [12] use a filtered velocity field to increase the reachable Taylor microscale Reynolds number. They use a low-pass filter on the velocity field and demonstrates that this method keeps the simplicity of implementing the linear forcing and allows the control of the Taylor microscale, which corresponds to controlling the integral length scale. In the work of Ketterl and Klein [9] another usage of a filtered velocity field can be found. The authors use the high-pass filtered velocity to control the integral length scale and turbulent kinetic energy fully. This approach offers the opportunity to study small-scale turbulence-flame interactions. Note that all of these works use cubic domains, which is not practical for researching flame fronts.

All of the above-discussed methods are developed for incompressible flows. Petersen and Livescu [13] show that the linear forcing method is capable of maintaining statistically stationary turbulence in a compressible flow. However, they also show that the original Lungren term is insufficient to control the ratio of dilatational to solenoidal kinetic energies and dissipation. Therefore a stationary state is not reachable. Petersen and Livescu propose splitting the forcing term, which needs a Fourier transformation of the flow field, making its application difficult on adapted grids. But Petersen and Livescu also report that at higher

turbulent Mach number (in [13] greater than $\mathrm{Ma}_t = 0.1$), the ratio becomes more stable, but the long-time behavior is difficult to be predicted. We observe equivalent results at higher Mach numbers, and the dilatational to solenoidal ratio is very stable. Several other authors research compressible turbulence, e.g. [5,8,18]. Most authors do not use a linear forcing approach and study turbulence in cubic domains with a fixed mesh. Independently from the specific forcing, there exists statistically turbulence properties, for example, in terms of Mach number scaling, which can be used as validation.

In this report, we investigate turbulence forcing for a rectangular domain with a locally adapted mesh. For the designated investigation of compressible turbulent flames, the control of the RMS-velocity and the integral length scale (independently of the domain size) of compressible turbulence is necessary. For this, a spatial forcing with a quick convergence to a stationary state combined with a real-space filter is proposed.

The paper is organized as follows. In Sect. 2, we give a short overview of the most important equations and implementation details. Section 3, presents different test cases and discusses the advantages and disadvantages of the linear forcing method for turbulence-flame interactions studies. To this end, we focus on the requirements in terms of usage of a rectangular domain with an adapted grid. Finally, Sect. 4 gives a short outlook to a few computations in preparation for future turbulence-flame interactions. We take a closer look at important statistical properties.

2 Basis Equations and Numerical Details

2.1 Governing Equations

We study isotropic turbulence in a compressible inert gas, which is governed by the three-dimensional compressible Navier-Stokes equations in skew-symmetric form [14]. These equations are

$$\begin{aligned}
\sqrt{\varrho}\partial_t\sqrt{\varrho} + \frac{1}{2}\partial_{x_i}\left(\varrho u_i\right) &= 0 \qquad (1)\\
\sqrt{\varrho}\partial_t\left(\sqrt{\varrho}u_i\right) + \frac{1}{2}\left(\partial_{x_j}\left(\varrho u_j u_i\right) + \varrho u_j \partial_{x_j} u_i\right) &= -\partial_{x_i} p + \partial_{x_j}\tau_{ij} + f_i\\
\frac{1}{\gamma-1}\partial_t p + \frac{\gamma}{\gamma-1}\partial_{x_i}\left(u_i p\right) &= \partial_{x_i}\left(\lambda\partial_{x_i} T\right) + u_i\partial_{x_i} p\\
&\quad - u_j\partial_{x_j}\tau_{ij} + \partial_{x_i} u_i\tau_{ij} + f_e,
\end{aligned}$$

with density ϱ, velocity u_i, pressure p, temperature T, thermal conductivity λ and heat capacity ratio γ. The viscous tensor is $\tau_{ij} = -\frac{2}{3}\mu\partial x_k u_k\delta_{ij} + \mu\left(\partial_{x_j} u_i + \partial_{x_i} u_j\right)$ and we use the equation of state for an ideal gas. f_i and f_e are the turbulent forcing terms and to ensure total energy conservation $f_e = -f_i u_i$, analogous to [13]. The skew symmetric scheme is fully conservative and fluxes can be defined [14], by which it becomes analogous to a FV scheme. Its shock treatment was validated [4,14] .

2.2 Linear Forcing

The original Lundgren [11] forcing term is defined by a constant A and the velocity field u_i

$$f_i = Au_i. \tag{2}$$

The parameter A is an adjustable parameter. Analyzing the stationary turbulent kinetic energy equation, one can identify that A depends on the specific properties of the turbulent field, hence $A = (2\tau)^{-1}$ with eddy-turnover time $\tau = \frac{k}{\varepsilon}$. Due to the choice of A, a specific turbulent state is selected. If for the integral length scale $l_t = 0.2L$ [15] (domain size L) is assumed, the turbulent target values k and ε can be calculated with a fixed viscosity ν. After that, the Kolmogorov length scale is determined, and the necessary grid resolution could be calculated.

Bassenne et al. [1] modified the forcing term as:

$$f_i = \frac{\varepsilon(t) - G(k(t) - k_0)/t_0}{2k(t)} u_i. \tag{3}$$

k_0 is the target value for the turbulent kinetic energy and t_0 is the constant integral time. The parameters k and ε are the current time-dependent values for the turbulent field. All target values can compute similarly to the described method above. G is a dimensionless constant to ensure that the turbulent kinetic energy approaches the target value exponentially [1]. Note that larger values of G produce faster convergence and less fluctuating turbulence target values, but lead to stiffer equations and, therefore, eventually smaller time steps in order to avoid numerical errors.

Another modification of Lundgren's linear forcing approach is proposed by Ketterl and Klein [9]

$$f_i = A\tilde{u}_i. \tag{4}$$

Instead of using the entire velocity field and therefore inject kinetic energy at all velocity modes, Ketterl and Klein use a high-pass filtered field $\tilde{u}_i$. It is computed as the difference $\tilde{u}_i = u_i - \hat{u}_i$, with a typically LES convolution filter $\hat{u}_i$. We combine in our work the forcing term from Bassenne et al. with a filtered velocity analogous to Ketterl and Klein, where $\hat{u}_i$ is computed with a box filter

$$\hat{u}_i = \frac{1}{(2L_f + 1)^3} \sum_{j=-L_f, L_f} u_i(x + j, y + j, z + j), \tag{5}$$

with filter width L_f. This filter is easy to implement and most importantly, due to the filter width, capable of working at different grid refinement levels.

2.3 Compressible Turbulence

One important characteristic of compressible turbulence is revealed when the Navier-Stokes equations are split into a solenoidal and dilatational part with the Helmholtz decomposition. Erlebacher et al. [7] concludes that the solenoidal part corresponds to the incompressible part of the equations. With increasing turbulent Mach number, the dilatational part becomes larger, and therefore compressible effects occur in the flow field. Sakar et al. [16] propose a way to decompose the turbulent dissipation ε into solenoidal and dilatational parts without a full Helmholtz decomposition:

$$\varepsilon = \varepsilon_s + \varepsilon_d = 2\mu\omega_{ij}\omega_{ij} + \frac{4}{3}\mu\left(\partial_{x_k} u_k\right)^2, \tag{6}$$

with $\omega_{ij} = \frac{1}{2}(\partial_{x_i} u_j - \partial_{x_j} u_i)$. This computation of the dissipation ε is necessary to calculate the correct turbulent dissipation rate to adjust the forcing term. The incompressible definitions can be used for all other specific turbulent parameters.

2.4 Technical Details

We use the code WABBIT, which is introduced in [17]. On the RHS subroutine, we discretize Eq. 1 with 4th order schemes in space and time. The time step is adapted to meet the CFL criterium. We use an adaptive shock filter [3] to treat shocks at higher turbulent Mach numbers.

Forcing terms and statistical properties of the flow field are easy to implement because all of these parameters can be computed locally, which means on single blocks. Therefore only a few and simple MPI communications are needed, for example, to gather the statistical data after the local computation. The box filtered velocity is computed only every $n > 50$ time steps, which is sufficient to obtain statistical stationary turbulence. Large filter widths L_f are implemented due to a loop with smaller filter widths and regular ghost nodes synchronization.

3 Test Cases

3.1 Linear Forcing in Cubic Domains

The Lundgren forcing term (Eq. 2) is an attractive first choice, and due to its simple implementation, especially for using with adapted grids and reactive Navier-Stokes equations. With the specific parameter A, the turbulent properties are well determined. The integral length scale l_t correlates with the domain size L [15], and therefore l_t can only change due to a change in L, restricting its applicability. Too small domain sizes are not possible in our designated application, since the domain needs at least a size of a few flame widths. Larger domain sizes are easier to implement in principle, especially with adapted grids. However, these domains still lead to increasing computational costs.

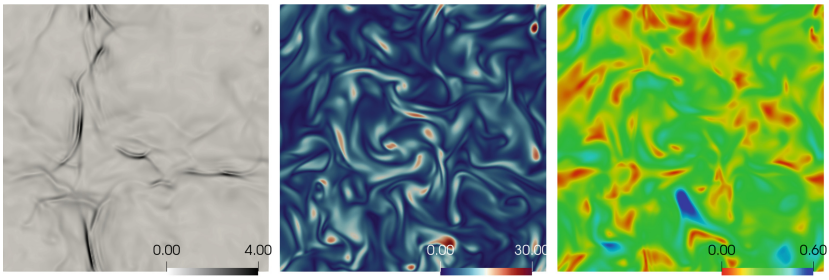

Fig. 2. Contour plots for a turbulent field with Lundgren forcing approach. (a) density gradient $\nabla\varrho$, (b) vorticity magnitude $|\omega|$, (c) local Mach Number Ma_{loc}, cubic domain $L = 2\pi$, resolution 256^3, fixed viscosity $\nu = 5.8\mathrm{e}{-3}$, $\mathrm{Re}_\lambda = 52$, $\mathrm{Ma}_t = 0.3$, $\varrho_0 = 1$, $p_0 = 16$

In Fig. 2 we show results for a classical Lundgren forcing case for a compressible regime. In the fluctuations of $\nabla\varrho$ shock-like structures dominate the flow field. The strongest shocks are not perfectly resolved, which can be seen from the oscillating (wave-like) structures in front of the shock. Note that this can be fixed by a stronger filtering. The vorticity ω (b) shows smoother structures than the density gradient. The size of these structures corresponds to the integral length scale of the flow. Typical structures like vortex kernels and filaments are well visible. In (c), the local Mach number is shown. The turbulent Mach number, which is calculated with the RMS-velocity, is for this case $\mathrm{Ma}_t = 0.3$. The local Mach number is due to velocity fluctuations much larger. For example from Fig. 11 one can observe, that locally a Mach number $\mathrm{Ma}_{loc} > 1$ is reached for a turbulent Mach number $\mathrm{Ma}_t > 0.3$.

As mentioned above, the linear forcing term can directly be used with adapted grids. A great benefit of this simple forcing term is the applicability to coarser grids, even for dynamically adapted grids, since the forcing parameter does not need to be changed for other grid levels. In Fig. 3 results for coarser grids are shown. It is worth noting that the target turbulent flow would not fit into the coarser grid, which means smaller scales simply not exist (well to observe in Fig. 3 (b–c)). But the statistical properties of the turbulent flow are well approximated, even though the filtering must be stronger for coarser grids. Note, that the modified term after Bassenne (Eq. 3) requires time-dependent values for k and ε. But these can be computed directly at a coarser mesh as well.

Figure 4 shows the time evolution of the statistical properties for $\tau = 60$ eddy-turnover times. The order of magnitude of the fluctuations corresponds to results in the literature. The very small fluctuation of the RMS-velocity u_{rms} for the Bassenne forcing term is clearly visible. The integral length scale l_t is

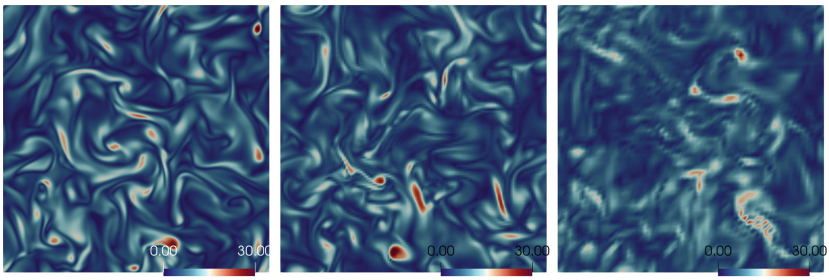

(a) (b) (c)

Fig. 3. Contour plots of vorticity magnitude $|\omega|$ for a turbulent field with Lundgren forcing approach. cubic domain $L = 2\pi$ with resolution (a) 256^3, (b) 128^3, (c) 64^3, fixed viscosity $\nu = 5.8\text{e}{-3}$, $\mathrm{Re}_\lambda = 52$, $\mathrm{Ma}_t = 0.3$, $\varrho_0 = 1$, $p_0 = 16$

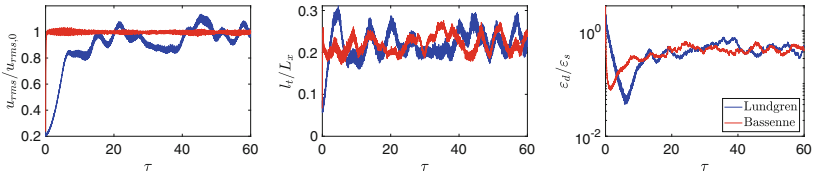

(a) (b) (c)

Fig. 4. Time evolution of important turbulent properties with Lundgren and Bassenne forcing approach. (a) RMS velocity u_{rms}, (b) integral length scale l_t, (c) ratio of dilatational to solenoidal dissipation $\frac{\varepsilon_d}{\varepsilon_s}$, cubic domain $L = 2\pi$ with resolution 256^3, fixed viscosity $\nu = 5.8\text{e}{-3}$, $\mathrm{Re}_\lambda = 52$, $\mathrm{Ma}_t = 0.3$, initial density $\varrho_0 = 1$, initial pressure $p_0 = 16$

approximately 0.2 of the domain size L. We observe for both methods (Lundgren, Bassenne) a constant ratio of solenoidal to dilatational dissipation if the turbulent Mach number is sufficiently large enough, as reported in [13]. Generally, in most cases, a constant ratio occurs with $\mathrm{Ma}_t > 0.1$.

With increasing turbulent Mach number, also the fluctuations increase, especially with the original Lundgren forcing term. This can be observed in Fig. 5(a), which shows the accuracy of achieving the target value of the Taylor microscale Reynolds number Re_λ over the turbulent Mach number. For very large Mach numbers $\mathrm{Ma}_t > 0.6$, these fluctuations further increase, and the flow field needs even more filtering. However this Mach number region is not attractive for our turbulence-flame interaction research, because for such large velocity fluctuations a spontaneous DDT could occur, and therefore we would need much more numerical/computational effort. (e.g. to resolve the detonation front) The energy spectra (Fig. 5(b)) show a sensible energy distribution over all modes and an excellent agreement between these two forcing methods.

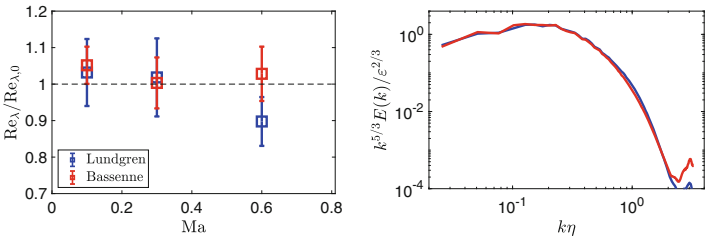

Fig. 5. Turbulent properties with Lundgren and Bassenne forcing approach. (a) Taylor microscale Reynolds number Re_λ, (b) normalized energy spectra, cubic domain $L = 2\pi$, resolution 256^3, fixed viscosity $\nu = 5.8\mathrm{e}{-3}$, $\mathrm{Re}_\lambda = 52$, $\mathrm{Ma}_t = 0.3$, initial density $\varrho_0 = 1$, initial pressure $p_0 = 16$

3.2 Linear Forcing in Rectangular Domains

For the study of flame fronts, a rectangular non-cubic domain is very advantageous. Even a laminar flame needs a specific domain size to reach a stationary state. Turbulent flames typically need even more space to statistically converge since the flame speed is difficult to predict and can thus not fully be compensated with an inflow condition. Pure cubic domains thereby yield high computational costs. Unfortunately, as reported in [10], the linear forcing fails to reach for rectangular domains a statistically stationary state. The impact on the flow field could be very complicated to predict. In some cases, a few properties are in good agreement with the cubic reference case, and therefore the flow field would seem correct. Generally, the non-stationary behavior becomes more apparent with more elongated domains.

In Fig. 6, as an example, the velocity component U_y is shown at different times. In some areas of the velocity field, the fluctuations seem meaningful. But even in the first figure, the dominance of a mode in the elongated direction is observed. And this mode is becoming more dominant over time. The energy spectra in Fig. 7(c) show that the energy is wrongly distributed, especially at the lowest wavenumbers. Due to the energy conservation, the increasing energy in lower wavenumbers leads to decreasing energy at higher wavenumbers, which is very disadvantageous in studying turbulence-flame interactions because the small scales can enter the flame, respectively the reaction zone, and therefore significantly affect the flame speed.

The time evolution of the forcing parameter A is shown in Fig. 7. Note that first A is assumed constant for calculating the necessary parameters in the forcing term in the RHS-subroutine. However, looking at the (with time-dependent k and ε) computed value of A, the difference between the two domain shapes can be observed. For a cubic domain, the target value is reached and fluctuates similarly

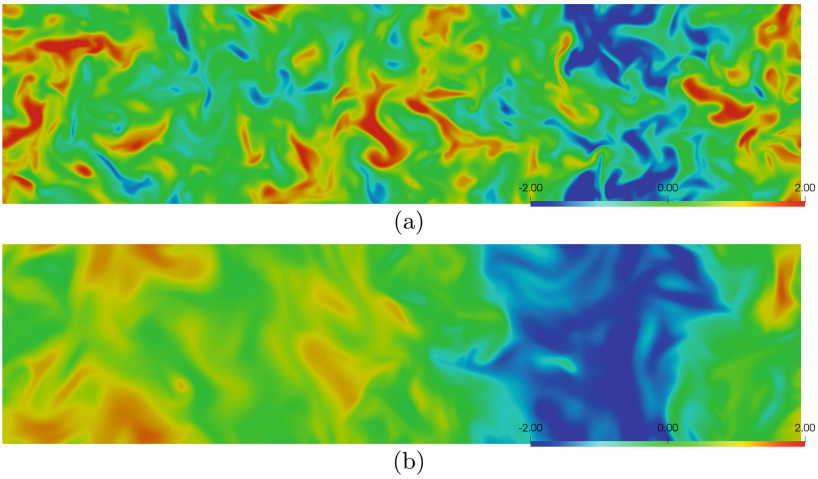

Fig. 6. Contour plots for velocity fluctuations u_y with Bassene forcing approach for a rectangular domain. (a) after $\tau = 10$ eddy-turnover times, (b) $\tau = 60$, rectangular domain 4:1. $L_y = 2\pi$ with resolution 1024×256^2, fixed viscosity $\nu = 5.8\text{e}{-3}$, $\text{Re}_\lambda = 52$, $\text{Ma}_t = 0.3$, initial density $\varrho_0 = 1$, initial pressure $p_0 = 16$

to all other turbulence properties. In a rectangular domain, on the other hand, the target value of A is missed. Additionally, even the ratio of solenoidal to dilatational dissipation decreases over time, which corresponds to an increasing solenoidal or decreasing dilatational part, which leads to less compressible effects in the flow field.

3.3 Linear Forcing with Box-Filtered Velocity in Rectangular Domains

One solution to reach a stationary and adequate turbulence, is the usage of a filtered velocity field for the forcing term. This approach is a usual method to control the integral length scale, especially when using Fourier space formulations. A sharp spectral filtered velocity, which removes the low wavenumber modes, works at fixed and equidistant grids. However, for a physical space solver, this method is not practical because of the high computational cost when transforming the entire velocity field into the Fourier space. Additionally, with an adapted mesh, the exact Fourier coefficient calculation is very expensive, maybe not affordable due to the computational limitations. It should be noted that an approximate computation of the Fourier transformation on the coarse grid did not solve the problem. From our experience, even a small part of any low wavenumber mode inside the forcing term leads to the above-described problem.

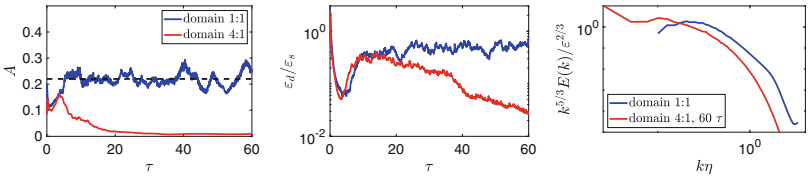

Fig. 7. Important turbulent properties with Bassenne forcing approach for a cubic/rectangular domain. (a) time evolution forcing parameter A, (b) time evolution ratio of dilatational to solenoidal dissipation $\frac{\varepsilon_d}{\varepsilon_s}$, (c) normalize energy spectra, rectangular domain 4:1. $L_y = 2\pi$ with resolution 1024×56^2, cubic domain accordingly, fixed viscosity $\nu = 5.8\text{e}{-3}$, $\text{Re}_\lambda = 52$, $\text{Ma}_t = 0.3$, initial density $\varrho_0 = 1$, initial pressure $p_0 = 16$

The integral length scale can be made smaller than 0.2 of the domain size L with a filtered velocity forcing term. This is an essential property concerning studying premixed turbulent combustion. Smaller integral length scales lead to higher Karlovitz numbers, which is, in general, a challenging field for research. Another significant advantage of this method (especially for the box-filtered method) is the fact that the filter works entirely locally. Therefore this forcing term can easily be used on adapted grids, without any Fourier space formulation. From a practical point of view, we can report that it is sufficient to filter the velocity field only every $n > 50$ time steps, which is essential when using large filter widths.

In Fig. 8 the results for different length scales in cubic domains with a non-adapted grid are shown. It is well observable that the turbulent structures and scales become smaller with decreasing integral length scales. This behaviour affects the vorticity kernels and the shock fronts, but generally, the vorticity magnitude and the shock strength increase with smaller length scales.

We find a linear correlation between the filter width L_f and the integral length scale l_t, which is shown in Fig. 9(b). In the energy spectra for the different filter widths, a decreasing integral length scale can be observed. If the turbulent Mach number is fixed for the different cases, then, due to a smaller integral length scale, one needs a finer grid (smaller Kolmogorov scale), and the Taylor microscale Reynolds number decreases. This is well visible in Fig. 9(c). From the time evolution of l_t (Fig. 9(a)) one can see that the statistical fluctuation is reduced for smaller length scales.

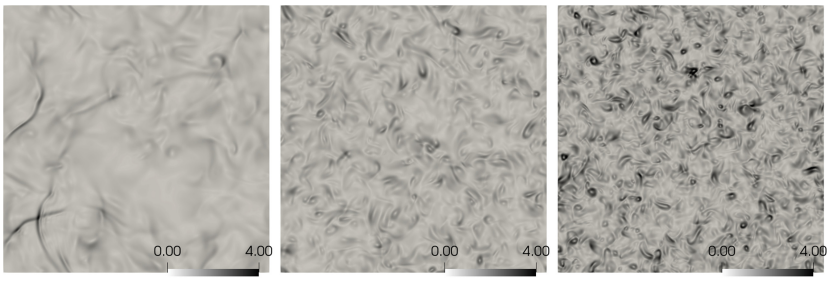

(a) (b) (c)

Fig. 8. Contour plots of density gradient $\nabla\varrho$ for a turbulent field with box filtered forcing approach. cubic domain $L = 2\pi$ (a) resolution 288^3, integral length scale $l_t = 0.8L_y$ at $\mathrm{Re}_\lambda = 41$, $L_f = 400$, (b) 416^3, $l_t = 0.2L_y$ at $\mathrm{Re}_\lambda = 21$, $L_f = 80$, (c) 512^3, $l_t = 0.1L_y$ at $\mathrm{Re}_\lambda = 15$, $L_f = 20$, fixed viscosity $\nu = 5.8\mathrm{e}{-3}$, $\mathrm{Ma}_t = 0.3$, initial density $\varrho_0 = 1$, initial pressure $p_0 = 16$

4 Results

Finally, we present the results of our work in preparation to compute turbulence-flame interaction for the setup of the specific pulsed detonation combustor (PDC). Grid resolution and domain size are adapted to the parameters of premixed H_2/air flames. The integral length scale l_t and the turbulent Mach number Ma_t are chosen to reasonable values. It is planned to vary these parameters to study different regimes and characteristic points inside the Borghi diagram. In the center of the domain is the region of the finest mesh, which is approximately 2x of the thermal flame thickness δ_{th}. (see Fig. 10) The box-filtered forcing term is active there to maintain the turbulent field. The grid is coarsened outside this area, following the restrictions and rules of our code [17]. For this example, we use a mesh with a compression rate of ≈0.976, which saves 97% of the grid nodes compared to the corresponding equidistant mesh at the finest grid level. The area at the finest grid level could be quickly too small from a practical view,

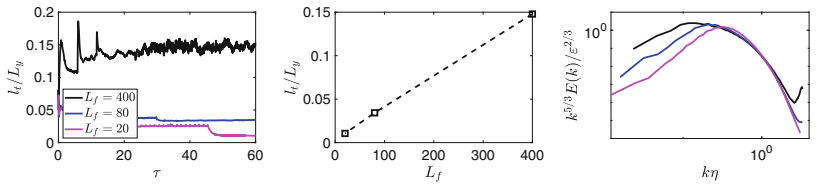

(a) (b) (c)

Fig. 9. Important turbulent properties with box filtered forcing approach for different filter widths L_f. cubic domain $L = 2\pi$ with resolution 256^3 (a) time evolution integral length scale l_t, (b) correlation l_t to L_f, (c) energy spectra, for $L_f = [400, 80, 20]$ with $\mathrm{Re}_\lambda = [41, 21, 15]$, fixed viscosity $\nu = 5.8\mathrm{e}{-3}$, $\mathrm{Ma}_t = 0.3$, initial density $\varrho_0 = 1$, initial pressure $p_0 = 16$

especially for a wide distributed broken flame front. However, in this situation, we can adapt the grid, and due to the large velocity fluctuations, the turbulence needs only a short time to move to the newly adapted most refined grid level, which can be observed when turbulence enters the coarsened area of the grid. The fine turbulent scales, which can not exist on the coarse mesh, are suddenly removed, and overall the turbulent kinetic energy decays after that. We observe large-scale structures at the coarse grid level, which can have locally large velocity fluctuations. However, this can be handled due to specific customized filter steps, e.g., an adaptive filtering [3] to control shocks.

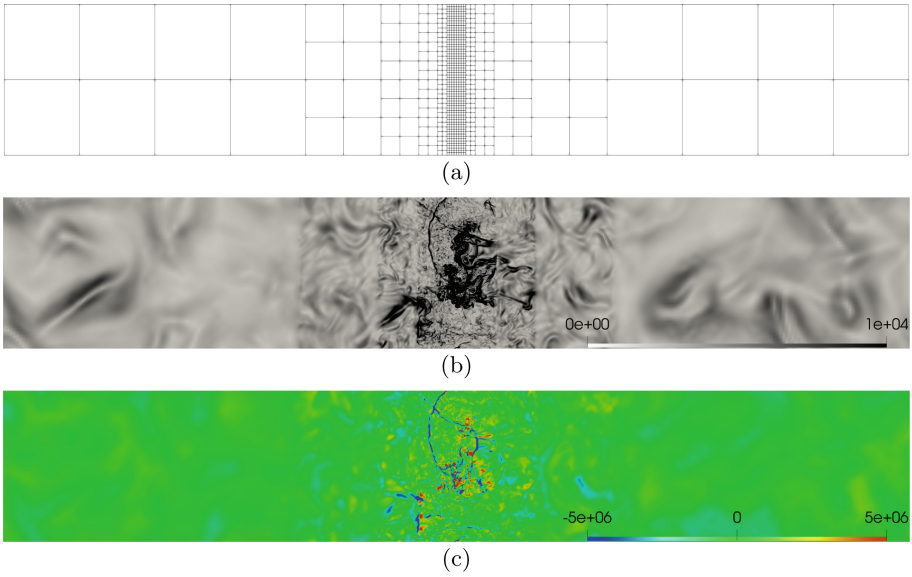

Fig. 10. Contour plots for a turbulent field with box filtered forcing approach in a rectangular domain (6:1) with an adapted grid. Domain $L_x = 12$ mm, $L_{y,z} = 2$ mm with block resolution 26^3, adaptation of 6 mesh levels (fixed mesh at level 6 corresponds to 9984×1664^2, compression rate $\approx$0.976), (a) grid, (b) density gradient $\nabla\varrho$, (c) velocity divergence Θ, fixed viscosity $\nu = 2.16\text{e}{-5}$, $\mathrm{Ma}_t = 0.4$, initial density $\varrho_0 = 0.85$, initial pressure $p_0 = 1$ bar, $l_t = 0.1L_y$, $\frac{\eta}{dx} = 1.03$

In the contour plots (Fig. 10), the different turbulent scales and structures can be seen. These flow characteristics are similar to the results from our test cases. Note that we choose the color bar scaling of the $\nabla\varrho$ to highlight the coarser parts of the grid. One can observe the decreasing magnitude of the density gradient from the finer mesh to the coarser level and also the disappearance of the small, turbulent scales. The velocity divergence contour plot is scaled to focus on the structures in the most refined mesh. The two typical flow field features, vorticity kernels and shock fronts can be observed in both plots. We do not show the time evolution of the turbulent properties, but these behave equivalent to the test

cases. Generally, the box-filtered forcing method works very well for an adapted grid. A statistical stationary state is quickly reached, and the numerical effort is noticeably reduced due to the mesh adaptivity. It is advantageous not to start with the most refined grid level, rather than using a coarser mesh overall and adapt this step by step. For that procedure, the filter width L_f is easy to adapt to different mesh levels.

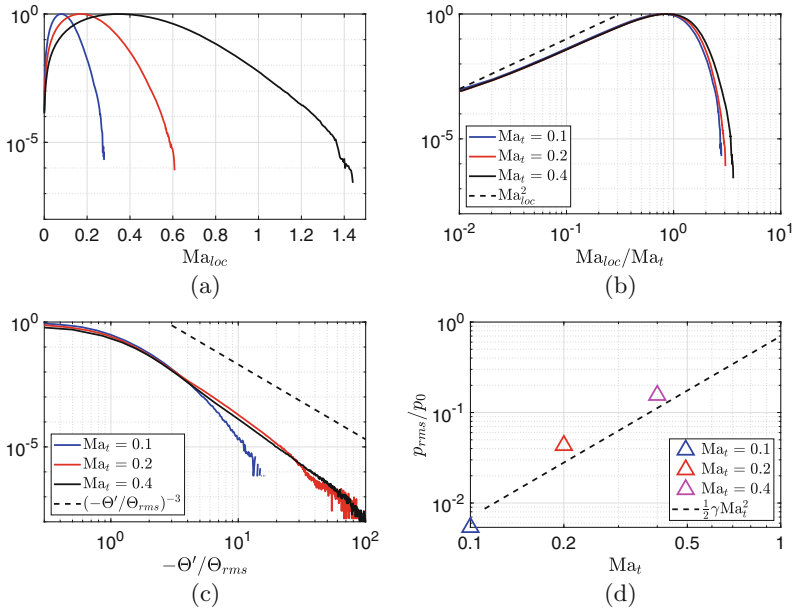

Fig. 11. Statistical properties for different turbulence fields with box filtered forcing approach in a rectangular domain, (a) PDF of local Mach number Ma_loc, (b) PDF of normalized local Mach number, (c) normalized velocity divergence Θ, (d) normalized RMS-pressure p_{rms} versus turbulent Mach number Ma_t

Different PDFs for computations of several turbulent Mach numbers are shown in Fig. 11. Excellent visible is the increasing local Mach number for increasing turbulent Mach number. Above $\mathrm{Ma}_t > 0.3$, the local Mach number becomes supersonic, according to the results from, e.g., [18]. The normalized Mach number curves collapse nearly to a single curve, and the values of $\mathrm{Ma}_{loc} < \mathrm{Ma}_t$ scales with Ma_t^2, which is also reported in the literature. Another statistically meaningful result can be observed for the normalized velocity divergence. The region of large divergence, which corresponds to the shock-like structures in the flow field, scales for $\mathrm{Ma} > 0.2$ with -3, similar to [18]. The pressure fluctuations are more significant for higher turbulent Mach numbers, and we observe (not shown), like in [8], an increase of the pressure fluctuations on the positive side for Mach numbers $\mathrm{Ma}_t > 0.2$. The RMS-pressure scales with Ma_t^2. Overall we see those important statistical properties correspond to results from

the literature, and therefore we can conclude that our forcing method can reach and maintain a physically meaningful compressible turbulent flow field at an adapted non-cubic grid.

5 Conclusions

We discussed the applicability of the linear forcing method to adapted locally refined grids in rectangular domains. Our test cases show that the standard linear forcing term cannot create and maintain a physically meaningful turbulent field, even for an equidistant (uniform) mesh. We observed a highly increased turbulent kinetic energy for the low-wavenumber modes, which cause especially an unsteady evolution of the turbulent properties. Further, the integral length scale is not controllable, a key parameter for turbulent flame investigations. A solution to the described problem is the use of a filtered velocity field inside the forcing term. We use the box-filtering approach, which is simple to implement. For this, we observed complete control of the integral length scale on an adapted grid. Finally, we show a statistically good evolved turbulent field in preparation for our future work.

We plan to study turbulence-flame interactions in regimes at high Karlovitz numbers and compressible Mach numbers for our further work. The preliminary work of this report will be helpful in the creation of the necessary turbulent flow fields.

Acknowledgment. The authors gratefully acknowledge the support of the Deutsche Forschungsgemeinschaft (DFG) as part of collaborative research center CRC 1029 (project 200291049) “Substantial efficiency increase in gas turbines through direct use of coupled unsteady combustion and flow dynamics”.

References

1. Bassenne, M., Urzay, J., Park, G.I., Moin, P.: Constant-energetics physical-space forcing methods for improved convergence to homogeneous-isotropic turbulence with application to particle-laden flows. Phys. Fluids **28**(3), 035114 (2016)
2. Bengoechea, S., Gray, J., Reiss, J., Moeck, J., Paschereit, O., Sesterhenn, J.: Detonation initiation in pipes with a single obstacle for mixtures of hydrogen and oxygen-enriched air. Combust. Flame **198**, 290–304 (2018)
3. Bogey, C., Cacqueray, N., Bailly, C.: A shock-capturing methodology based on adaptative spatial filtering for high-order non-linear computations. J. Comput. Phys. **228**, 1447–1465 (2009)
4. Brouwer, J., Reiss, J., Sesterhenn, J.: Conservative finite differences as an alternative to finite volume for compressible flows. In: Fuhrmann, J., Ohlberger, M., Rohde, C. (eds.) Finite Volumes for Complex Applications VII-Methods and Theoretical Aspects, pp. 169–176, Springer International Publishing, Cham (2014). https://doi.org/10.1007/978-3-319-05684-5_15
5. Campos, A., Morgan, B.: The effect of artificial bulk viscosity in simulations of forced compressible turbulence. J. Comput. Phys. **371**, 111–121 (2018)

6. Carroll, P., Blanquart, G.: A proposed modification to Lundgren's physical space velocity forcing method for isotropic turbulence. Phys. Fluids **25**, 5114 (2013)
7. Erlebacher, G., Hussaini, M., Sarkar, S., Kreiss, H.: The analysis and simulation of compressible turbulence. Theoret. Computat. Fluid Dyn. **2**, 2 (1990)
8. Jagannathan, S., Donzis, D.A.: Reynolds and mach number scaling in solenoidally-forced compressible turbulence using high-resolution direct numerical simulations. J. Fluid Mech. **789**, 669–707 (2016)
9. Ketterl, S., Klein, M.: A novel turbulent inflow data generation method and its application to the simulation of primary breakup. In: Salvetti, M.V., Armenio, V., Fröhlich, J., Geurts, B.J., Kuerten, H. (eds.) Direct and Large-Eddy Simulation XI. ES, vol. 25, pp. 229–235. Springer, Cham (2019). https://doi.org/10.1007/978-3-030-04915-7_31
10. Klein, M., Chakraborty, N., Ketterl, S.: A comparison of strategies for direct numerical simulation of turbulence chemistry interaction in generic planar turbulent premixed flames. Flow Turbul. Combust. **99**, 12 (2017)
11. Lundgren, T.: Linearly forced isotropic turbulence. Center Turbul. Res. Ann. Res. Briefs **2003**, 02 (2003)
12. Palmore, J.A., Desjardins, O.: Technique for forcing high reynolds number isotropic turbulence in physical space. Phys. Rev. Fluids **3**, 034605 (2018)
13. Petersen, M.R., Livescu, D.: Forcing for statistically stationary compressible isotropic turbulence. Phys. Fluids **22**(11), 116101 (2010)
14. Reiss, J., Sesterhenn, J.: A conservative, skew-symmetric finite difference scheme for the compressible Navier-Stokes equations. Comput. Fluids **101**, 08 (2013)
15. Rosales, C., Meneveau, C.: Linear forcing in numerical simulations of isotropic turbulence: physical space implementations and convergence properties. Phys. Fluids **17**(9), 095106 (2005)
16. Sarkar, S., Erlebacher, G., Hussaini, M.Y., Kreiss, H.O.: The analysis and modelling of dilatational terms in compressible turbulence. J. Fluid Mech. **227**, 473–493 (1991)
17. Sroka, M., Engels, T., Krah, P., Mutzel, S., Schneider, K., Reiss. J.: An open and parallel multiresolution framework using block-based adaptive grids. In: King, R. (ed.) Active Flow and Combustion Control 2018, pp. 305–319, Springer International Publishing, Cham (2019)
18. Wang, J., Gotoh, T., Watanabe, T.: Shocklet statistics in compressible isotropic turbulence. Phys. Rev. Fluids **2**, 023401 (2017)